NJC

ROYAL SOCIETY OF CHEMISTRY

PAPER

View Article Online
View Journal

Cite this: DOI: 10.1039/c9nj05466a

Effects of different plasticizers on highly crosslinked NaAlg/PSSAMA membranes for pervaporative dehydration of *tert*-butanol

Divya D. Achari, Satishkumar R. Naik and Mahadevappa Y. Kariduraganavar *

Received 1st November 2019,
Accepted 9th February 2020

DOI: 10.1039/c9nj05466a

rsc.li/njc

Polystyrene sulfonic acid-*co*-maleic acid (PSSAMA) crosslinked sodium alginate (NaAlg) membranes were developed by incorporating diethyl phthalate (DEP), dibutyl phthalate (DBP) and dioctyl phthalate (DOP). The physico-chemical properties of the resulting membranes were studied using FTIR, WXRD, TGA, DSC, AFM and SEM techniques. Before the membranes were subjected to pervaporation studies, the membranes' sorption studies were carried out in different compositions of water/*tert*-butanol. The effects of the different plasticizers on their pervaporation performance were investigated systematically for the separation of water/*tert*-butanol mixtures at different temperatures. Among the membranes, the membrane containing DEP exhibited the highest separation factor of 12 830 with a flux of 1.306 × 10^{-3} kg m^{-2} h^{-1} for 10 mass% water in the feed. The total flux and the flux of water were found to overlap with each other, indicating that the developed DEP incorporated membrane could be used effectively to break the azeotropic point of water/*tert*-butanol. The activation energy obtained for the permeation of water (E_{pw}) was significantly lower than that of *tert*-butanol (E_{pTER}), suggesting that the DEP incorporated NaAlg/PSSAMA membrane had a higher separation ability and thus demonstrated excellent performance in the dehydration of *tert*-butanol. The heat of sorption (ΔH_s) of all the membranes was found to be negative, indicating that Langmuir's mode of sorption is predominant.

Introduction

Pervaporation (PV) is considered as an efficient and environmentally friendly membrane separation technique with several advantages, such as low energy consumption, high selectivity and simple design, as compared to conventional separation processes.[1–3] The working principle of PV is mainly based on the molecular separation of liquid mixtures in which a membrane surface is equilibrated in a feed solution and as a consequence some of the components can pass through the membrane and can be collected as vapors in the permeate. Thus, PV is a process with tremendous potential for separating azeotropes and close-boiling mixtures.[4–7] It is considered as the most promising membrane technology for the separation of aqueous *tert*-butanol mixtures.[8,9] *tert*-Butanol is a short chain alcohol that is being used as a solvent in most of the chemical and pharmaceutical industries. It is also used as a raw material in the production of artificial musks, synthetic perfumes and denatured alcohols. Thus, dehydration of *tert*-butanol has a high demand in both academia and industry.

For the dehydration of water/*tert*-butanol mixtures, hydrophilic membranes are preferred in order to achieve high permeability, good selectivity and sufficient mechanical strength.[10–12] In view of this, many hydrophilic polymers including poly(vinyl alcohol),[13,14] polyimides,[15] sodium alginate[16,17] and polyelectrolytes[18–20] have been reported as PV membrane materials. Many researchers have designed a large number of polymeric membranes for the recovery of *tert*-butanol from its azeotropic mixtures. For instance, An *et al.*[21] prepared and characterized the behavior of Matrimid® 5218 polyimide membranes for pervaporation separation of 85% aqueous *tert*-butanol at 60 °C and achieved a flux of 965 g m^{-2} h^{-1} with a separation factor of 491. Zhang *et al.*[22] prepared poly(acrylic acid) (PAA)/polyethyleneimine self-assembled hollow fiber polyelectrolyte multilayer membranes and they achieved a separation factor of 481 with a flux of 769 g m^{-2} h^{-1} at 50 °C. Kalyani *et al.*[23] developed a sodium alginate and hydroxyethylcellulose blend membrane for the dehydration of *tert*-butanol and obtained a flux of 2300 g m^{-2} h^{-1} with a separation factor of 3237.

Sodium alginate being a natural polysaccharide has demonstrated an excellent performance as a PV membrane material for the dehydration of water–alcohol mixtures.[24] Its carbohydrate chains consist of sugar moieties which contain a large number of carboxyl groups and hydroxyl groups, providing exceptional hydrophilicity to the NaAlg membrane and excellent permselectivity nanochannels for water.[25] However, the higher hydrophilicity of NaAlg leads to

Department of Chemistry, Karnatak University, Dharwad – 580 003, India.
E-mail: mahadevappayk@gmail.com, kariduraganavarmy@kud.ac.in

its instability in aqueous solution during the PV process. Apart from its water solubility, the lower mechanical properties of the NaAlg membrane are considered to be disadvantageous for its potential use in the PV process.[26] Therefore, many attempts have been made towards improving the mechanical properties of NaAlg membranes for better PV performance. Among them, crosslinking is considered as one of the most promising modification methods.[27,28] Thus, the crosslinking method has been extensively used by researchers to modify sodium alginate membranes in order to achieve thermal stability and good selectivity.

For instance, Xie *et al.*[29] prepared NaAlg-perfluorinated sulfonic acid (PFSA)/ceramic hybrid membranes, wherein the membrane with 2 wt% NaAlg and 2 wt% PFSA demonstrated the highest flux of 1155 g m^{-2} h^{-1} with a separation factor of 1149 for the dehydration of 15 wt% water content in an ethanol–water mixture at 75 °C. Zhang *et al.*[30] fabricated polyelectrolyte multilayer composite membranes by depositing chitosan and NaAlg solutions alternatively onto a hydrolyzed porous poly(acrylonitrile) (PAN) substrate. The resulting composite membranes exhibited a separation factor of 4491 with a flux of 596 g m^{-2} h^{-1} for the dehydration of 90% water/isopropanol mixtures at 60 °C. Thus, it was greatly supported by studies that crosslinking would integrate the chemical structure and stabilizes the polymeric chains of NaAlg membranes.[31] However, a serious drawback of crosslinking lies in the difficulty in regulating the crosslinked chemical reaction, which affects the degree of crosslinking and thus impacts the membrane performance.[32,33] On the other hand, excessive crosslinking leads to the brittleness of the polymeric membranes with the loss of dimensional stability, thereby making them unsuitable for PV applications. Rachipudi *et al.*[34] reported polyelectrolyte complex membranes of NaAlg by crosslinking with PSSAMA for the separation of water/1,4-dioxane mixtures. It was observed that the membranes became brittle and lost their required properties for higher amounts of PSSAMA (>75 mass%) crosslinking agent.

To circumvent the problems of NaAlg and PSSAMA, plasticizers could play an important role in altering the mechanical properties of a brittle polymer membrane. The plasticizer introduced into the polymeric macromolecules influences the chain mobility and thus increases the flexibility of the chains, and thus affects the permeability of small molecules. The influence of plasticizers on polymeric materials was investigated by some of the researchers.[35,36] However, the effects of plasticizers on the membrane properties and their influences on the transport of azeotropic mixtures in the PV process have not been studied in the literature.

Understanding the above mentioned problems, we made an attempt to incorporate plasticizers into PSSAMA crosslinked NaAlg membranes. Briefly, optimum amounts of three different plasticizers, such as diethyl phthalate, dibutyl phthalate and dioctyl phthalate, were incorporated into highly crosslinked NaAlg/PSSAMA membranes. The physico-chemical properties of the resulting membranes were studied with different techniques, and their PV performances were evaluated at different temperatures and feed compositions. The performances of the membranes were discussed by correlating the separation factor and permeation flux values with the structures of the plasticizers. From the temperature dependences of the permeation fluxes and the diffusion coefficients, the Arrhenius activation parameters were determined. The results were discussed in terms of the PV separation efficiency of the membranes.

Experimental

Materials

Tertiary butanol (*tert*-butanol) and sodium alginate (NaAlg) were procured from S. D. Fine Chemicals Ltd, Mumbai, India. Polystyrene sulfonic acid-*co*-maleic acid (sodium salt) (M_w = 20 000), dioctyl phthalate (M_w = 390.564 g mol^{-1}), dibutyl phthalate (M_w = 278.34 g mol^{-1}) and diethyl phthalate (M_w = 222.24 g mol^{-1}) were procured from Sigma-Aldrich, USA. All the chemicals were of reagent grade and used without further purification. Water was deionized and distilled before use.

Membrane preparation

Sodium alginate (4 g) was dissolved in 100 ml of distilled water followed by the addition of 3.2 wt% PSSAMA under constant stirring for 24 h. The resulting viscous, homogenous solution was spread onto a glass plate with the aid of a casting knife in a dust-free atmosphere. It was then allowed to dry at room temperature for about 2–3 days. The completely dried crosslinked NaAlg membrane was subsequently peeled-off and was designated as SP-0. The preparation of the crosslinked NaAlg/PSSAMA membrane is presented in Scheme 1.

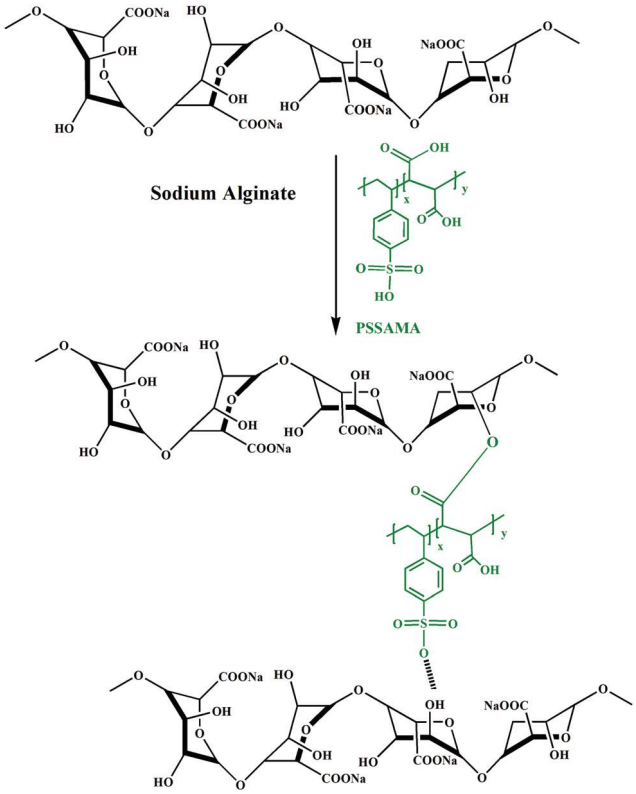

Scheme 1 Schematic representation of a highly crosslinked NaAlg/PSSAMA (SP-0) membrane.

To the above crosslinked homogenous solution, 6 wt% diethyl phthalate was added under constant stirring for 3 h. The resulting solution was poured onto a clean glass plate and the membrane was dried and designated as SPDEP. Similarly, 6 wt% dibutyl phthalate and 6 wt% dioctyl phthalate were separately incorporated into NaAlg/PSSAMA membranes and were, respectively, designated as SPDBP and SPDOP. The amounts of NaAlg and crosslinker were kept constant for all the membranes. Further, all the membranes were annealed at 110 °C for 3 h. We also made an attempt to incorporate more than 6 wt% DEP and DOP plasticizers into the crosslinked membranes, but in all the cases, we obtained full oily surfaced membranes due to phase separation between the plasticizer and membrane material. Thus, we restricted to only 6 wt% plasticizers in all the membranes. The thicknesses of the membranes were measured at different points using a Peacock dial thickness gauge (Model G, Ozaki Mfg. Co. Ltd, Japan) with an accuracy of ±2 μm, and the average thickness was considered for calculation. The thicknesses of the membranes were found to be 40 ± 2 μm in all the cases. The preparation of the different plasticizer incorporated PSSAMA crosslinked NaAlg membranes is shown in Scheme 2.

To elucidate the structures of the PSSAMA crosslinked NaAlg membrane and its plasticizers incorporated crosslinked membranes, we performed Molecular Modeling (Schrodinger, Maestro Software) with Disorder System and Molecular Dynamics Simulation studies to obtain the crosslinked structure of the NaAlg/PSSAMA membrane and possible interactions that occurred between NaAlg/PSSAMA and the different plasticizers, and the resulting structures are presented in Fig. 1. Briefly, all the molecules built for the simulation were converged with a 6-31G** hybrid B3LYP basis set with a cut off radius of 9 Å at the Density Functional Theory (DFT) level.[37] Further, the molecular dynamics were run with *NPT* at 300 K with 1.013 bar.

Characterization studies

The chemical crosslinking and interaction of the SP-0, SPDEP, SPDBP and SPDOP membranes were analyzed using a FTIR spectrometer (Nicolet, Impact 410, USA) within a range from 400 to 4000 cm^{-1}. To evaluate the changes in the intensities of the peaks in each scan, the amounts of membrane samples and KBr were kept constant. The changes in the crystallinities of the plasticized membranes were evaluated using a wide-angle X-ray diffractometer (Bruker, D-8 Advance, USA) equipped with a Cu Kα radiation source at 40 kV and 30 mA. The 2θ scanning range was operated in a transmission mode from 10 to 60° with a scanning speed of 2° min^{-1}. The thermal behavior of the plasticized membranes was investigated using a thermogravimetric analyzer (Model SDT Q600, TA Instruments, PerkinElmer TGA/DTA, USA). The samples with weights ranging from 6 to 9 mg were heated at 10 °C min^{-1} from ambient temperature to 600 °C under a nitrogen atmosphere. The glass transition and melting temperatures of the membranes were analyzed using a differential scanning calorimeter (DSC Q 20, TA Instruments, Waters LLC, USA) at a heating rate of 10 °C min^{-1} under a nitrogen atmosphere. The surface morphologies of the membranes were studied using an atomic force microscope (Nanosurf, Model easyScan 2 Flex AFM, USA) and a scanning electron microscope

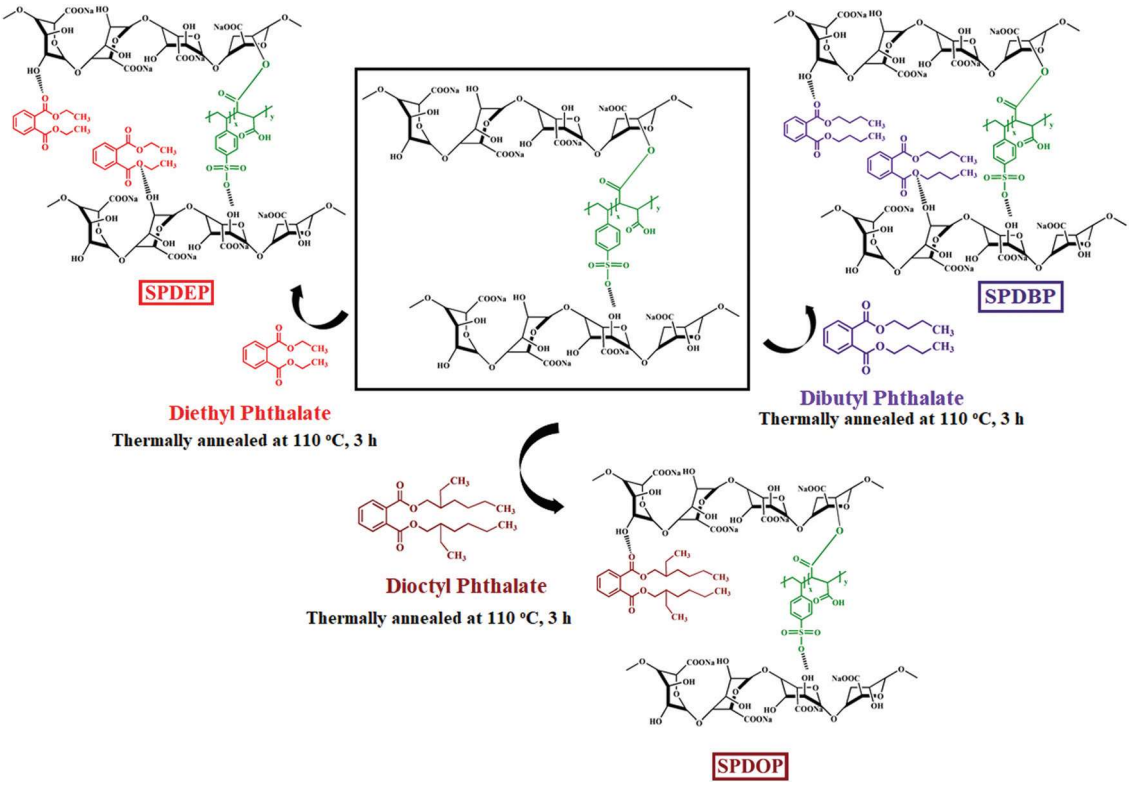

Scheme 2 Scheme for the preparation of different plasticizer incorporated crosslinked NaAlg/PSSAMA membranes (SPDEP, SPDBP and SPDOP).

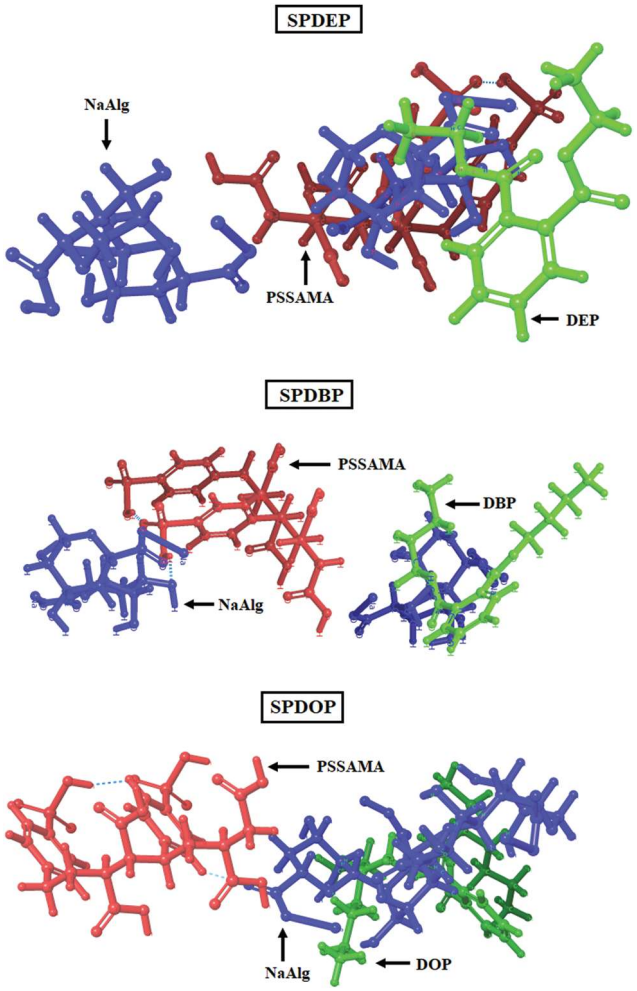

Fig. 1 The crosslinked structures of different plasticizer incorporated crosslinked NaAlg/PSSAMA membranes (SPDEP, SPDBP and SPDOP).

(JEOL, JSM-6390LV, Japan) at an accelerating voltage of 5 kV. The tensile strengths of the membranes were measured using a universal testing machine (Lloyd LRX plus, New Delhi, India) equipped with a 5 kN load cell. The membrane was fixed vertically between two pairs of grips with a length of 10 cm. The membrane was then extended at a constant elongation rate of 25 mm min^{-1} until it was broken. The hydrophilicities of the membranes were measured by the sessile drop method *via* a contact angle instrument (Kyowa Contact Angle Meter, Model DMS-401, Japan) at room temperature. A drop of distilled water was set on the surface of the membrane and Image analysis software was used to measure the contact angle.

Degree of swelling

To perform swelling experiments, the dried samples of all the membranes were weighed and immersed in different compositions of water/*tert*-butanol mixtures. Each sample was weighed periodically (for every 30 min) until no weight change was observed. The constant swelling weights were obtained after 3 h, which ensured that the swollen plasticized membranes reached an equilibrium state. The swollen membranes were removed and weighed (after the superfluous liquid was wiped out with tissue paper) in a digital microbalance (Mettler, B204-S, Toledo, Switzerland) with an accuracy of ±0.01 mg. The results were averaged after performing all the tests at least three times. The percent degree of swelling (DS) was calculated as shown in eqn (1):

$$\mathrm{DS}\,(\%) = \left(\frac{W_s - W_d}{W_d}\right) \times 100 \qquad (1)$$

where W is the mass of the membrane. Subscripts s and d refer to the swollen and dry membranes, respectively.

After performing the liquid sorption test, the amount of sorption in the membrane was calculated using eqn (2).[38] Finally, a sorption curve that shows an uptake of solvent *versus* the square root of time was plotted.

$$\frac{M_t}{M_\infty} = Kt^n \qquad (2)$$

where M_t is the actual mass uptake at time t; M_∞ is the final mass uptake; K is a constant incorporating characteristics of the polymer system and penetrant; and n is the diffusion coefficient, which is an indicator of the transport mechanism.

Pervaporation experiments

The PV performance of the resulting membranes was investigated using an indigenously designed laboratory-scale pervaporation setup as shown in our previous paper.[39] Briefly, the effective membrane surface area in contact with the feed mixture was 34.23 cm^2 and the capacity of the feed compartment was about 250 cm^3. A two-stage vacuum pump (Toshniwal, Chennai, India) was used to keep the vacuum [1.333224×10^3 Pa (10 Torr)] on the downstream side of the apparatus. The membranes were enabled to equilibrate for 3 h, in a feed compartment with different compositions which varied from 5 to 25 mass% water in water/*tert*-butanol mixtures, before performing the PV. Once the membranes attained equilibrium, permeate was collected in a trap submerged in a liquid nitrogen jar on the downstream side. The experiments were carried out at 30, 40 and 50 °C. The collected permeate was weighed on a digital microbalance to evaluate the flux and separation factor. The compositions of water and organic solvents in the permeate were assessed by determining the refractive index (RI) of the permeate with an accuracy of ±0.0001 unit using Abbe's refractometer (Atago-ST, Tokyo, Japan) and by comparing it with a standard graph of the refractive index, which was previously established with the known composition of water/*tert*-butanol. All the experiments were conducted at least three times and the results were averaged. The results of the azeotropic mixtures during the course of PV were reproducible within the permissible range. The separation performance of the membranes was evaluated in terms of the total flux (J), separation factor (α_{sep}) and pervaporation separation index (PSI). These parameters were calculated, respectively, using the following equations:

$$J = \frac{W}{A \cdot t} \qquad (3)$$

$$\propto_{sep} = \frac{P_w/P_{org}}{F_w/F_{org}} \quad (4)$$

$$PSI = J(\propto_{sep} - 1) \quad (5)$$

where W is the mass of the permeate (kg); A is the membrane area (m^2); t is the permeation time (h); P_w and P_o are the respective mass fractions of water and organic solvent in the permeate; and F_w and F_o are the mass fractions of water and organic solvent in the feed, respectively.

Further, the permeance (P_i/l) was calculated using eqn (6). Based on the permeance, the intrinsic properties of the membranes were evaluated:[40,41]

$$\frac{P_i}{l} = \frac{D_i K_i}{l} = \frac{J_i}{P_i^f - P_i^p} \quad (6)$$

where D_i and K_i are the diffusion and sorption coefficients of the ith component, respectively; P_i is the permeability of the ith component; P_i^f and P_i^p are the vapor pressures of the ith component in the feed and permeate, respectively; l is the membrane thickness; and j_i is the molar flux of the ith component.

Results and discussion

Fourier-transform infrared spectroscopy (FTIR)

FTIR spectra of NaAlg/PSSAMA (SP-0) and different plasticizer incorporated NaAlg/PSSAMA membranes (SPDEP, SPDBP and SPDOP) are shown in Fig. 2. The interactions were ascertained by frequency shifting or band broadening of specific functional groups.[42] Pure NaAlg exhibited a broad and strong band at 3400 cm^{-1}, which corresponded to the stretching vibrations of the hydroxyl groups. The bands appearing at 1609 and 1412 cm^{-1} were assigned to the symmetric and asymmetric stretching of C=O groups, respectively.[34] After the incorporation of a higher amount of PSSAMA into the NaAlg matrix, the bands were shifted to higher wavenumbers. Briefly, the bands at (i) 3426, (ii) 1617 and 1412, (iii) 1027, and (iv) 1120 cm^{-1} were, respectively, corresponded to the (i) O–H stretching vibrations, (ii) asymmetric and symmetric C=O stretching, (iii) symmetric S=O groups and (iv) asymmetric S=O groups. The presence of DEP in the NaAlg/PSSAMA membrane (SPDEP) was noticed by three significant bands: 1732 cm^{-1} related to C=O stretching, 1280 cm^{-1} assigned to conjugated aromatic ester R–COOR groups and 2988 cm^{-1} attributed to the –CH stretching frequency.[43] In the SPDOP membrane, the presence of DOP was confirmed by the strong absorption bands related to C–O stretching ranging between 1100 and 1300 cm^{-1} and C=O stretching appearing at 1732 cm^{-1}.[44] In the SPDBP membrane, the presence of DBP was confirmed by the appearance of characteristic absorption bands at 1122 cm^{-1} for C–O stretching,[45] 1722 cm^{-1} for C=O stretching and 1598 cm^{-1} for –CH– stretching with respect to the aromatic nucleus of the DBP. All these observations indicate that there was a good compatibility between the plasticizer and NaAlg/PSSAMA matrix, which could lead to good PV performance.

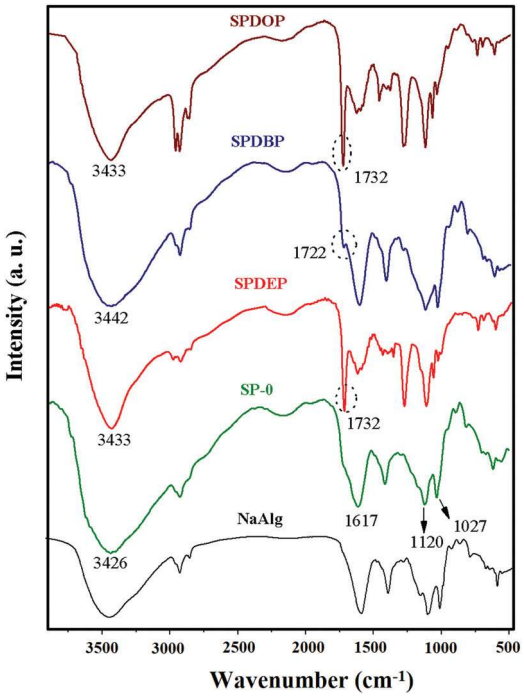

Fig. 2 The FTIR spectra of NaAlg, SP-0, SPDEP, SPDBP and SPDOP membranes.

Wide angle X-ray diffraction (WXRD)

To study the effects of the different plasticizers on the crystallinity of NaAlg/PSSAMA membranes, X-ray diffraction study was carried out for all the membranes, and the resulting patterns are shown in Fig. 3. According to the literature, the diffraction pattern of pure sodium alginate exhibits characteristic peaks at around 13.4°, 19°, 22.7°, 28°, 28.9°, 32.5° and 33.5°.[46,47] The relative intensities of the characteristic peaks of pure NaAlg

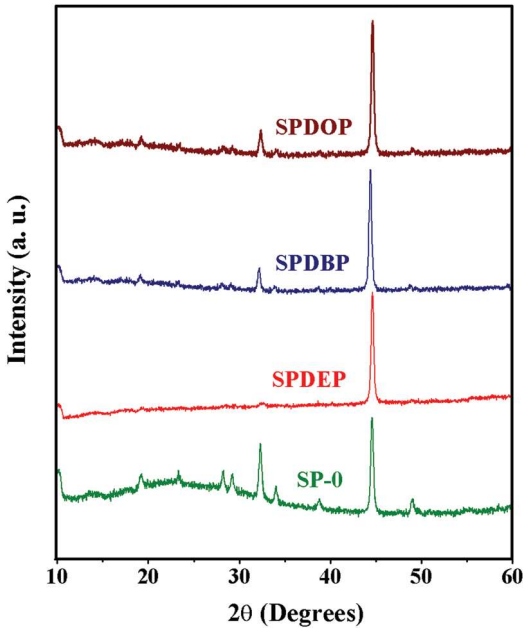

Fig. 3 The WXRD patterns of SP-0, SPDEP, SPDBP and SPDOP membranes.

were increased after the incorporation of a higher amount of PSSAMA into the polymer matrix (SP-0), which was attributed to the mixture of crystalline and amorphous regions. In addition to this, a new characteristic diffraction peak occurred at 45° due to the incorporation of PSSAMA content and this indicates the crystalline phase of the NaAlg/PSSAMA membrane. Further, it was observed that the incorporation of the different plasticizers into the highly crosslinked NaAlg/PSSAMA matrix enhanced the amorphous domain in the membrane matrix. In particular, the intensities of the peaks that appeared at 19°, 32.5° and 33.5° gradually decreased. In the case of the DEP incorporated NaAlg/PSSAMA membrane, these peaks had almost disappeared. This is due to the increased amorphous region and chain flexibility, which together contributes to the transport of small molecules (preferably water molecules) through the membrane. The higher amorphous proportion facilitates the segmental mobility and enhances the flexibility of the membrane.

Thermal properties

Thermogravimetric analysis (TGA). The thermal stability and degradation behavior of the NaAlg/PSSAMA membrane and different plasticizer incorporated NaAlg/PSSAMA membranes were investigated by TGA under nitrogen flow, and the resulting patterns are presented in Fig. 4. The thermal degradation behavior of all the membranes could be divided into three distinct stages which are associated with the thermal solvation, thermal desulfonation and thermal oxidization of polymer chains.

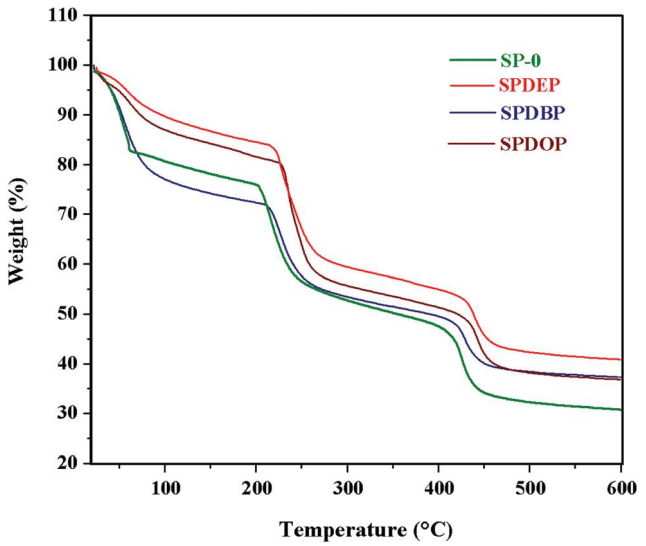

Fig. 4 The TGA thermograms of SP-0, SPDEP, SPDBP and SPDOP membranes.

From the first, second and third stages of decomposition temperatures and the total weight losses of all the membranes are tabulated in Table 1. The first stage of degradation occurred between 35 and 120 °C, which was attributed to the desorption of physically absorbed water molecules.[48] The second stage of major degradation occurred at around 200–350 °C with 36–44% weight loss. This is due to the molecular desulfonation in the membranes, which was correspondingly increased in the plasticizer incorporated membranes. The plasticizer, which was entrapped in the polymer matrix, formed a strong interaction between the oxygen of the plasticizer and polymer matrix. Thus, more energy was needed to interrupt the interactive bonds and thus lead to higher decomposition temperature.[49] In the case of the SPDOP membrane, the first and second stages of decomposition temperatures are lower than those of the SPDEP and SPDBP membranes. This may be due to the steric hindrance caused by the bulky groups (alkyl chains) on the ester oxygen, which inhibited the reactivity of the ester oxygen. The third stage of decomposition occurred beyond 350 °C due to the decomposition of the main polymer chains and the plasticizers. Based on these observations, it can be concluded that the incorporation of the plasticizers has greatly improved the thermal stability of NaAlg/PSSAMA owing to the establishment of interaction between the polymer and plasticizer.

Differential scanning calorimetry (DSC). The effects of the different plasticizers on the glass transition temperature (T_g) of NaAlg/PSSAMA membranes were determined by DSC. The DSC patterns of the highly crosslinked NaAlg/PSSAMA (SP-0) and different plasticizer incorporated membranes were recorded from ambient temperature to 400 °C, and the patterns thus obtained are presented in Fig. 5. From the literature, it is found that pure NaAlg exhibited T_g and T_m at around 81 and 230 °C, respectively.[50] It is revealed by the DSC patterns that the highly PSSAMA crosslinked NaAlg membrane with a stiff backbone exhibited high T_g and T_m of around 104 and 238 °C, respectively. This is due to the formation of a large number of hydrogen bonds between PSSAMA and NaAlg, which showed wide transition as can be seen from the thermogram. This broad transition cannot be considered or compared with the dehydroxylation or evaporation of moisture from the polymer.[50] From the literature, it is well understood that both T_g and T_m shift to lower temperatures upon adding the plasticizer content to the membrane matrix, whereas in this study the three different plasticizer incorporated membranes (SPDOP, SPDBP and SPDEP) had T_g and T_m values of around 102, 86 and 77 °C and 235, 231 and 227 °C, respectively. The decrease in T_g indicates that the plasticizers were readily miscible in the NaAlg/PSSAMA matrix, which further created space between

Table 1 Decomposition temperatures and total weight loss% of SP-0, SPDEP, SPDBP and SPDOP membranes

Membrane	1st decomposition temp. (°C)	2nd decomposition temp. (°C)	3rd decomposition temp. (°C)	Total weight loss (%)
SP-0	107.39	236.75	438.99	67.44
SPDEP	119.27	267.59	451.49	57.96
SPDBP	125.62	264.25	441.20	62.31
SPDOP	109.25	263.98	457.31	62.31

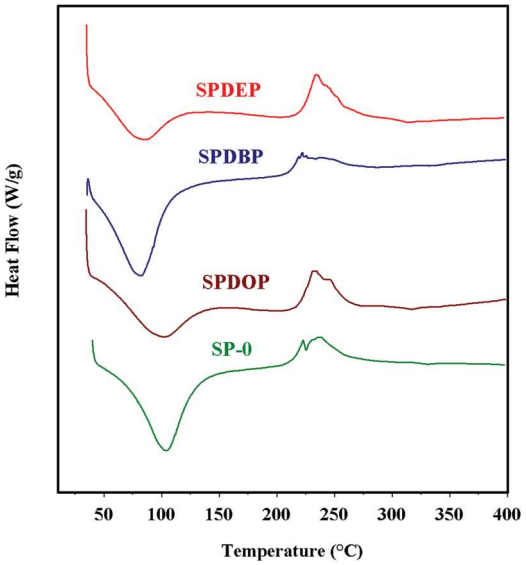

Fig. 5 The DSC thermograms of SP-0, SPDEP, SPDBP and SPDOP membranes.

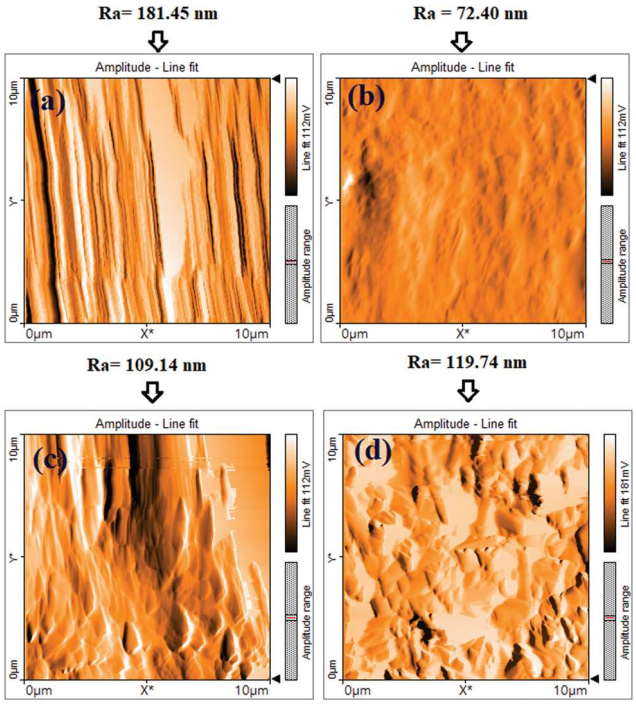

Fig. 6 The AFM images of membranes: (a) SP-0; (b) SPDEP; (c) SPDBP and (d) SPDOP.

the polymer chains due to the insertion of the plasticizers at the interstitial site and thus increased the free-volume, leading to flexibility in the membrane.[51] Among all the membranes, a relatively larger reduction in T_g was achieved by the SPDEP membrane owing to the smaller size of the DEP plasticizer.

Membrane morphology

Atomic force microscopy (AFM). Atomic force microscopy analysis revealed a possible correlation between the average roughness (R_a) and membrane hydrophilicity. Fig. 6 shows the AFM images of the membrane surfaces over a scan area of 10 µm × 10 µm. In the literature, it is reported that the increased hydrophilicity of the membrane could lead to a higher water content in the polymer matrix, and thus leads to an enhanced flexibility of the membranes, and thus decreased the roughness of the surface (R_a).[52] The highly crosslinked NaAlg/PSSAMA (SP-0) membrane showed a surface roughness of 181.45 nm. After incorporating the different plasticizers in the highly crosslinked NaAlg/PSSAMA matrix, the surface roughness was greatly reduced. Upon comparing the different plasticizer incorporated membranes, the DEP containing membrane showed a lower surface roughness value (72.40 nm) due to the large number of interactions between the oxygen atoms of DEP and the –OH groups of NaAlg. All these results signify that the addition of the plasticizers into the highly crosslinked membrane matrix (NaAlg/PSSAMA) enhanced the hydrophilicity of the membranes.

Scanning electron microscopy (SEM)

To assess the miscibilities and morphologies of the membranes, scanning electron microscopy was employed. Fig. 7(A and B) illustrates the SEM images of the surface and cross-sectional views of the NaAlg/PSSAMA and different plasticizer incorporated NaAlg/PSSAMA membranes. From the images, it can be seen that the surface of the SP-0 membrane was rough and relatively dense due to the presence of a higher amount of PSSAMA content in the membrane matrix. However, the addition of the plasticizers such as DEP, DBP and DOP creates a porous morphology on the surface of the membrane. The porous surface of the membrane plays a significant role in the permselectivity and has strict control over the membrane performance. In particular, the SPDOP membrane exhibited numerous large pores on its surface due to the large bulky structure of the DOP plasticizer, as compared to SPDEB and SPDBP. Fig. 7(B) presents the cross-sectional views of SP-0, SPDEP, SPDBP and SPDOP. From the image of SP-0, it is found that membrane was smooth without any macro-defects such as cracks. Also, the cross-sectional views of the SPDEP, SPDBP, and SPDOP membranes clearly showed sponge like structures. Thus, it can be concluded that the incorporation of the plasticizers not only improved the processability of the polymer matrix, but also created free-volume in the membrane matrix.

Mechanical properties

In PV, a membrane is kept in a cell at atmospheric pressure on its upstream side, while very low pressure is maintained on its downstream side. Thus, apart from the chemical resistance, the membrane should also have sufficient mechanical stability to maintain the constant differential pressure created across the membrane. There should be a proper balance between tensile strength, stability and membrane elongation in order to obtain good mechanical strength. The effects of the different plasticizers on the tensile strength and percent elongation of the crosslinked membrane were studied, and the data thus obtained are summarised in Table 2. The stress–strain curves of the resulting membranes are presented in Fig. 8.

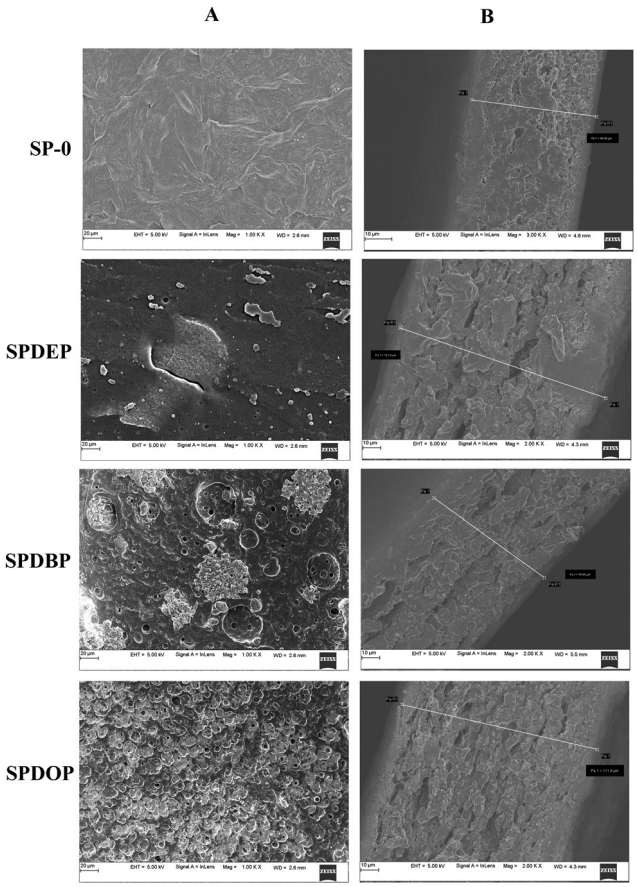

Fig. 7 The SEM images of SP-0, SPDEP, SPDBP and SPDOP membranes: (A) surface views and (B) cross-sectional views.

Table 2 Mechanical properties of SP-0, SPDEP, SPDBP and SPDOP membranes

Membrane	Tensile strength (MPa) (±5.0%)	Young's modulus (MPa)	Elongation at break (%) (±3.0%)
SP-0	123.96	5.233	33
SPDEP	70.87	1.495	53
SPDBP	80.21	2.148	43
SPDOP	105.74	3.401	39

It was observed that the highly crosslinked NaAlg/PSSAMA (SP-0) membrane exhibited a higher Young's modulus value of 5.233 MPa with a lower elongation at break of 33% due to its brittle nature. The incorporation of the plasticizers in NaAlg/PSSAMA membranes improved their flexibility and softness. As a result, the values of elongation at break increased for the SPDOP, SPDBP and SPDEP membranes as compared to the SP-0 membrane. However, upon incorporating the plasticizer, the tensile strength of the membrane decreased, and accordingly, it decreased from 123.96 to 105.74, 80.21, and 70.87 MPa for the SPDOP, SPDBP and SPDEP membranes, respectively. In particular, a maximum elongation at break was obtained for the SPDEP membrane. This can be attributed to the lower molecular weight of the DEP plasticizer, which allowed the movement of the plasticizer into the bulk of the polymer matrix. Thus, it created

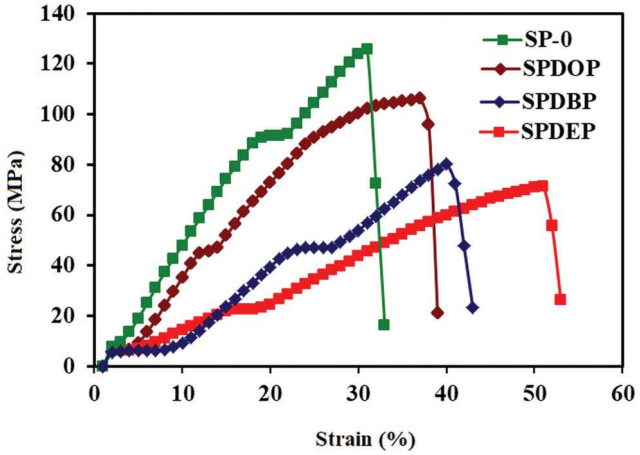

Fig. 8 The stress–strain curves of SP-0, SPDEP, SPDBP and SPDOP membranes.

effective plasticization in contrast to the higher molecular weight plasticizers DBP and DOP.[53]

Contact angle measurement

In order to examine the hydrophilicity of the resulting membranes, the water contact angles of the membranes were measured, and the values are presented in Fig. 9. It can be clearly seen that the contact angle of the highly crosslinked NaAlg/PSSAMA (SP-0) membrane was 49.6°. With the addition of the different plasticizers into the NaAlg/PSSAMA membrane, the contact angle values of the DOP, DBP and DEP incorporated membranes were found to be 44.3°, 38.6° and 34.9°, respectively, signifying that the developed plasticizer incorporated membranes exhibited excellent hydrophilicity. This is due to the higher amorphous nature of the plasticizer incorporated membranes, which facilitates their segmental mobility and hence enhances their flexibility. Among the membranes studied, the SPDEP membrane exhibited the lowest contact angle. This is due to the creation of extensive interactions (hydrogen bonding) between the oxygen atom (carbonyl oxygen of DEP)

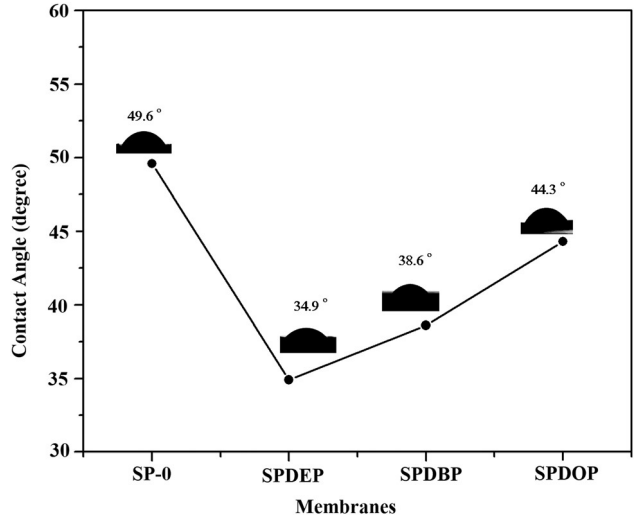

Fig. 9 The contact angles of SP-0, SPDEP, SPDBP and SPDOP membranes.

having two lone pairs of electrons and the –OH groups of NaAlg. There are relatively fewer interactions in the SPDOP membrane because of the steric hindrance caused by the bulky groups (alkyl chains) on the ester oxygen, and therefore hindered the reactivity of the ester oxygen and reduced the hydrophilicity of the SPDOP membrane.

Swelling study

In PV, membrane sorption plays a key role in the separation performance of the membrane,[54] which is generally assessed by the swelling capacity of the membrane in different feed mixtures. Fig. 10 shows the swelling behavior of all the membranes in different compositions of water/*tert*-butanol mixtures at 30 °C. It was observed that the degree of swelling increased almost linearly for all the membranes upon increasing the water composition in the feed. It could be concluded that the water/*tert*-butanol molecules were absorbed by the hydrophilic groups, such as C=O, –O–(alkyl group) and –OH, in the membranes and thus facilitated the transport of the molecules through the membranes. It is also observed that the plasticizer incorporated membranes showed greater degrees of swelling than the crosslinked NaAlg/PSSAMA membrane (SP-0). This is mainly attributed to the loosening of rigidity in the NaAlg/PSSAMA polymer membrane and thus increased free-volume. Upon comparing the degrees of swelling of the different plasticizer incorporated membranes, the DOP incorporated membrane exhibited the highest degree of swelling. This is mainly attributed to the bulky structure of DOP. This was clearly evidenced in the SEM images.

The sorption of solvents in the membrane matrix was also evaluated using sorption curves. The sorption curves for the highly crosslinked NaAlg/PSSAMA (SP-0) and different plasticizer incorporated membranes determined in different mass% of water in the feed at 30 °C are presented in Fig. 11. It is observed that the amount of sorption was increased upon increasing the mass% of water in the feed. This is due to the increased hydrophilic interactions between water molecules and the membrane. All these data support that the plasticizer incorporated membranes (SPDEP, SPDBP and SPDOP) exhibit more hydrophilicity than the highly crosslinked NaAlg/PSSAMA (SP-0) membrane.

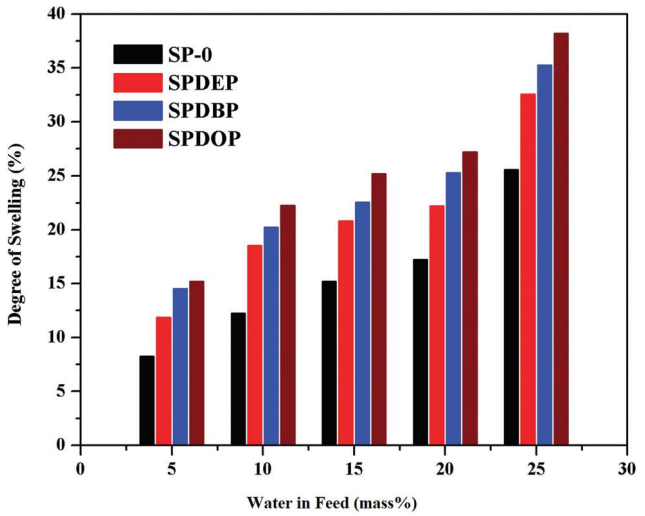

Fig. 10 The degrees of swelling of SP-0, SPDEP, SPDBP and SPDOP in different mass% of water in the feed.

Pervaporation study

Effects of feed composition and plasticizers on PV performance. The variations in the permeation flux by the addition of the different plasticizers into NaAlg/PSSAMA membranes determined at 30 °C for different feed compositions of water/*tert*-butanol are presented in Fig. 12. It was observed that the permeation flux was increased upon increasing the water content in the feed. This is due to the increased interaction between the membrane and feed mixture. In the PV process, the overall permeation flux and separation factor of the membrane are generally explained on the basis of three possible interactions, between the membrane and water, the membrane and alcohol, water and alcohol. When the first two interactions are stronger, due to the greater affinity between the permeants and the membrane, water or *tert*-butanol will be sorbed into the membrane. If the interaction between water and *tert*-butanol is strong, it leads to a coupling transport which increases the flux, while suppressing the separation factor. A simple method was employed to assess the material interaction based on the difference in the solubility parameter. The solubility parameters ($MPa^{1/2}$) of water, *tert*-butanol and NaAlg are 23.4, 10.6 and 29.6–36.1, respectively.[55,56] The difference in solubility parameter of each pair follows the order: *tert*-butanol/membrane > water/*tert*-butanol > water/membrane. This states that the water and membrane have the strongest interaction since they have the closest solubility parameter as compared to the other two sets. Consequently, the water content not only affects the membranes' swelling, but also favors the water transportation across the membrane.

In contrast to the swelling study, the SPDEP membrane showed the highest flux due to extensive hydrogen bonding interactions between the oxygen atom (carbonyl oxygen), the ester oxygen of DEP and the –OH groups of NaAlg. Although the swelling behaviour of the SPDOP membrane was high, the permeation of molecules through the membrane was less. This may again be attributed to the steric hindrance caused by the bulky groups (alkyl chains) on the ester groups of DOP in the polymer matrix. Further, in the case of highly crosslinked NaAlg/PSSAMA (SP-0), the membrane becomes fragile and is prone to mechanical failure due to high crosslinking, and thus we could not perform the PV experiment.

Fig. 13 describes the effects of mass% of water in the feed and plasticizers on the separation factor of all the membranes. It is observed that the separation factor was increased from 5 to 10 mass% and then decreased upon increasing the mass% of water in the feed. The same trend was observed for all the membranes. At higher mass% of water (15 to 25 mass%) in the feed, the membranes swell greatly owing to the greater interaction between the membrane and water molecule. Thus, the separation factor was decreased significantly at higher water compositions in the feed.

Similar to permeation flux, the DEP containing NaAlg/PSSAMA membrane exhibited the highest separation factor. This is due to

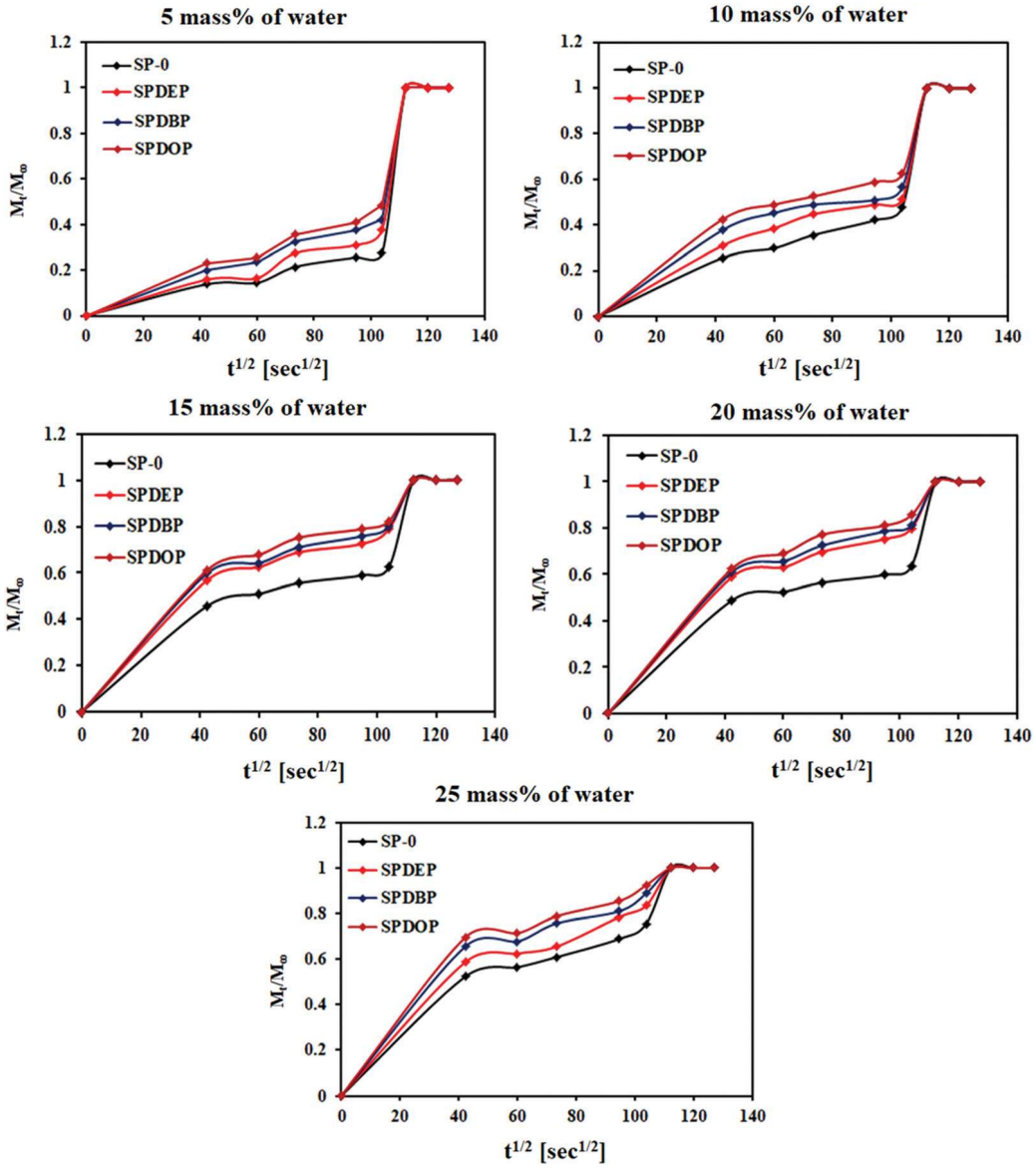

Fig. 11 The sorption curves of SP-0, SPDEP, SPDBP and SPDOP membranes in different mass% of water in the feed.

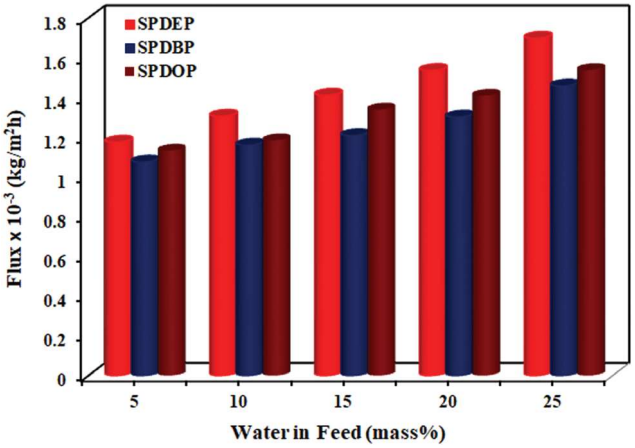

Fig. 12 Variation of total flux for SPDEP, SPDBP and SPDOP membranes with different mass% of water in the feed.

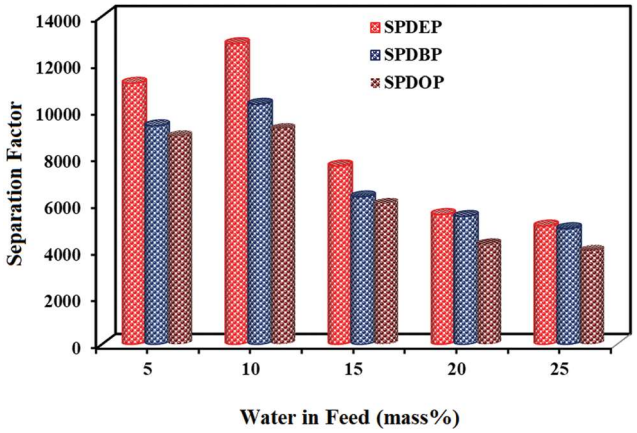

Fig. 13 Variation of separation factor for SPDEP, SPDBP and SPDOP membranes with different mass% of water in the feed.

the establishment of greater interactions between the oxygen atoms (carbonyl oxygen) of DEP and the –OH groups of sodium alginate. On the other hand, the DOP containing NaAlg/PSSAMA membrane exhibited the lowest separation factor owing to the bulky structure of DOP and created a porous structure, and thus led to the permeation of water and *tert*-butanol. Further, it is noticed that the permeation flux and separation factor values of all membranes were increased simultaneously up to 10 mass% of water in the feed and this is how; the trade-off phenomenon generally exists between the flux and separation factor was overcome by incorporating the plasticizers into the membrane matrix.

To evaluate the extent of permeation of individual components, we plotted the total flux, and the fluxes of water and *tert*-butanol for the different plasticizer incorporated membranes for 10 mass% water in the feed as shown in Fig. 14. From the plots, it is observed that the total flux and the flux of water are close to each other and are significant particularly for the DEP incorporated membrane, while the flux of *tert*-butanol was negligibly small for all the membranes, suggesting that the membranes developed in the present study by the incorporation of plasticizers are highly selective towards water.

In order to determine the membrane separation ability and assess the overall efficiency of the membranes, the pervaporation separation index (PSI) was calculated, and the values are plotted for the different plasticizer incorporated membranes for 10 mass% water in the feed (Fig. 15). From the graph, it is noticed that the DEP incorporated NaAlg/PSSAMA membrane showed the highest PSI value. This is due to the lower molecular weight of DEP in the framework of the membrane, which has not only changed the flexibility, morphology and hydrophilicity of the membrane, but also allowed the movement of the plasticizer into the bulk of the polymer matrix and made the plasticization more efficient compared to the higher molecular weight plasticizers, such as DBP and DOP.

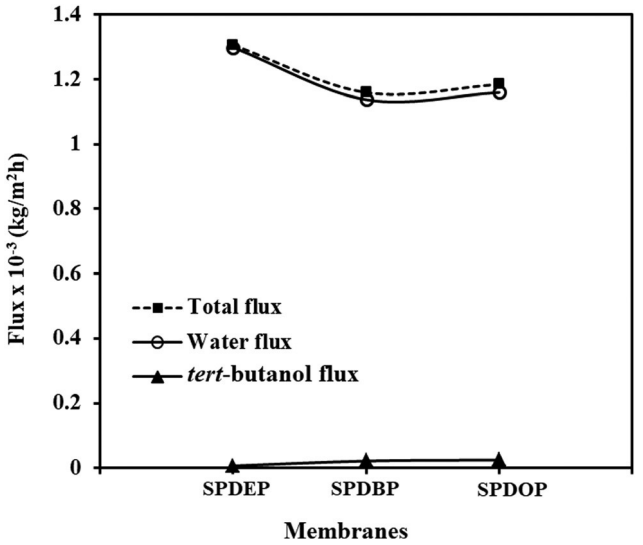

Fig. 14 Effects of different plasticizers on the total flux, and the fluxes of water and *tert*-butanol at 10 mass% water in the feed.

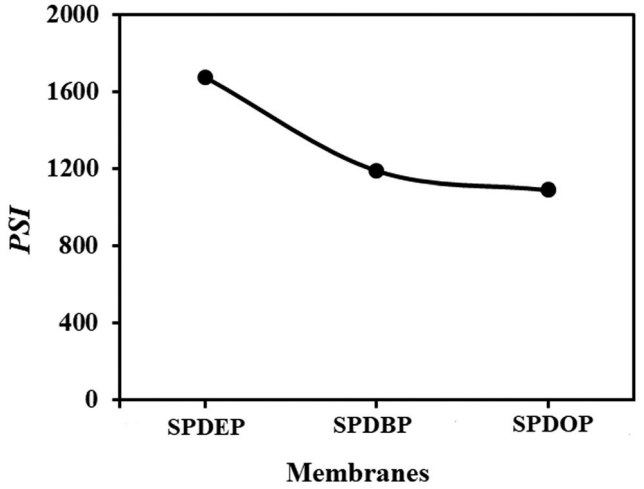

Fig. 15 Variation of pervaporation separation index for different plasticizer incorporated NaAlg/PSSAMA membranes at 10 mass% water in the feed.

The permeance is the key model parameter that was determined at different mass% of water in the feed. The calculated permeance values for the different plasticizer incorporated NaAlg/PSSAMA membranes in different mass% of water in the feed at 30 °C are presented in Table 3. From the table, it can be clearly seen that all the membranes exhibited greater water permeance as compared to *tert*-butanol, suggesting that the developed membranes are highly selective towards water molecules.[57] Among the membranes, the DEP incorporated NaAlg/PSSAMA membrane showed the highest water permeance and an improved separation factor at 10 mass% of water in the feed. From this, we concluded that the sorption of molecules into the polymer matrix is not only based on selectivity, but also on the size of permeants, since the kinetic diameter of *tert*-butanol (0.60 nm) is larger than that of water (0.265 nm). Thus, a larger amount of energy is required for *tert*-butanol as compared to water to diffuse through the SPDEP membrane containing lower molecular size DEP. This makes the plasticization more efficient and tends to be more hydrophilic by the creation of small free-volume and thus enhances the permeation flux and separation factor.

Permeability represents the intrinsic transport property of a material to a penetrant. The water permeability was calculated using eqn (7).[58]

$$P_w = \bar{P}_w \times L \quad (7)$$

Table 3 Permeance of water and *tert*-butanol at 30 °C for different plasticizer incorporated membranes at different mass% water in the feed

	P_w/l (GPU)			P_{TBA}/l (GPU)		
Mass% water	SPDEP	SPDBP	SPDOP	SPDEP	SPDBP	SPDOP
5	2936	2681	2827	2.62	2.72	3.17
10	3264	2897	2959	2.28	2.38	2.89
15	3529	3017	3347	2.77	2.54	3.29
20	3837	3252	3522	4.99	5.44	6.04
25	4158	3358	3699	5.58	6.23	7.56

GPU = gas permeation unit = 10^{-6} cc (STP) cm^{-2} s^{-1} cm^{-1} Hg^{-1}.

Table 4 Permeabilities of water and *tert*-butanol at 30 °C for different plasticizer incorporated membranes at different mass% of water in the feed

Mass% of water	Water permeability (1×10^{-4} Barrer)			*tert*-Butanol permeability (1×10^{-7} Barrer)		
	SPDEP	SPDBP	SPDOP	SPDEP	SPDBP	SPDOP
5	1.17	1.07	1.13	0.10	0.10	0.12
10	1.30	1.15	1.18	0.09	0.09	0.11
15	1.41	1.20	1.33	0.11	0.10	0.13
20	1.53	1.30	1.40	0.19	0.21	0.24
25	1.66	1.34	1.47	0.22	0.24	0.30

where L is the membrane thickness (cm) and P_w is the water permeability in units of Barrer = 1×10^{-10} cm^3 (STP) cm^{-1} (cm^{-2} s^{-1} $cmHg^{-1}$).

The estimated permeability values are presented in Table 4. The results are in good agreement with the flux data given in Fig. 12. According to Table 4, the highest water permeability and the lowest *tert*-butanol permeability values were observed for all the plasticizer incorporated NaAlg/PSSAMA membranes. This suggests that the plasticizer incorporated membranes are highly selective towards water. Among the membranes, the DEP incorporated NaAlg/PSSAMA membrane showed the highest water permeability with less permeability of *tert*-butanol at all water compositions in the feed. This clearly suggested that the DEP incorporated membrane is highly selective towards water owing to the interaction between lower molecular size DEP and the membrane matrix.

Diffusion coefficients. The solution diffusion mechanism plays an important role in understanding the PV process. According to this mechanism, the PV process involves three consecutive steps: sorption of the permeant from the feed side of the membrane, diffusion of the permeant across the membrane, and desorption of the permeant on the downstream side of the membrane.[59] Thus, the permeation rate and separation factor are governed by the solubility and diffusivity of each component of the feed mixture to be separated. However, during the process, the diffusion step controls the transport of penetrants owing to the establishment of fast equilibrium distribution between the bulk feed and the upstream surface of the membrane. Therefore, it is obviously important to estimate the diffusion coefficients of penetrating molecules in order to understand the mechanism of molecular transport. From Fick's law of diffusion, the diffusion coefficient can be expressed as shown in eqn (8):[60]

$$J_i = -D_i \frac{dC_i}{dx} \quad (8)$$

where J is the permeation flux per unit area (kg m^{-2} s^{-1}), D is the diffusion coefficient (m^2 s^{-1}), C is the concentration of permeant in the membrane (kg m^{-3}), subscript i indicates water or organic solvent, and x is the diffusion length (m). For simplicity, it is assumed that the concentration profile along the diffusion length is linear, and thus the diffusion coefficient D_i can be calculated with the following modified equation:[61]

$$D_i = \frac{J_i \delta}{C_i} \quad (9)$$

Table 5 Diffusion coefficients of SPDEP, SPDBP and SPDOP for water/*tert*-butanol at different mass% of water in the feed

Mass% of water	$D_w \times 10^8$ (cm^2 s^{-1})			$D_{TBA} \times 10^9$ (cm^2 s^{-1})		
	SPDEP	SPDBP	SPDOP	SPDEP	SPDBP	SPDOP
5	15.8	13.3	14.4	0.173	0.189	0.209
10	19.4	16.5	18.4	0.083	0.093	0.106
15	27.3	24.1	24.7	0.102	0.105	0.123
20	51.0	46.3	49.0	0.114	0.118	0.135
25	56.2	48.5	52.6	0.126	0.132	0.148

where δ is the thickness of the membrane. The calculated values of D_i at 30 °C are presented in Table 5.

It is observed that the diffusion coefficient of water was much higher than the diffusion coefficient of *tert*-butanol. Among the membranes studied, the DEP incorporated membrane exhibited the highest diffusion coefficient of water as compared to the other plasticizer incorporated membranes. This suggests that the membrane developed in the present study by the incorporation of DEP has demonstrated an excellent separation ability for the separation of water from *tert*-butanol. As discussed in the PV study, this was attributed to the increased hydrophilicity, selective adsorption and establishment of hydrogen bonding.

Temperature effect on PV performance. Temperature is an important operating parameter in the pervaporation process as it greatly induces the sorption and diffusion. The effect of operating temperature on the PV performance for water/*tert*-butanol mixtures was studied for all the membranes at 10 mass% of water in the feed, and the values thus obtained are presented in Table 6.

It is observed that the permeation rate was increased from 30 to 50 °C for all the membranes, while suppressing the separation factor. Generally, this happens for two reasons. First, as the temperature increases, the vapor pressure difference between the upstream and the downstream of the membrane increases, and this in turn enhances the driving force for the transport. Second, an increase of temperature promotes the thermal motion of polymer chain segments, creating more free-volume in the polymer matrix. However, in the present study, the latter reason is ruled out since the PV experiments were performed well below the glass transition temperature of NaAlg/PSSAMA. Therefore, the vapour pressure difference played a major role in transporting the associated molecules along with the selective permeants. This resulted in an increase of total permeation flux while suppressing the separation factor. Thus, the temperature dependence of permeation and diffusion

Table 6 Pervaporation fluxes and separation factors for all the membranes at 10 mass% of water in the feed

Temp. (°C)	$J \times 10^{-3}$ (kg m^{-2} h^{-1})			α_{sep}		
	SPDEP	SPDBP	SPDOP	SPDEP	SPDBP	SPDOP
30	1.306	1.160	1.185	12 830	10 252	9202
40	1.649	1.367	1.528	4274	4256	3323
50	1.749	1.457	1.604	3885	3207	3192

has prompted us to calculate the activation energy using the Arrhenius type equation:

$$X = X_0 \exp\left(\frac{-E_x}{RT}\right) \quad (10)$$

where X represents permeation (J) or diffusion (D), X_0 is a constant representing a pre-exponential factor of J_o or D_o, E_x denotes the activation energy for permeation or diffusion depending on the transport process under consideration, R is a gas constant, and T is the temperature (K).

Arrhenius plots of log$J$ and log$D$ *versus* temperature are shown in Fig. 16 and 17, respectively. In both the cases, a linear trend was observed, suggesting that the permeability and diffusivity follows an Arrhenius trend.

We estimated the activation energies for total permeation (E_p) and total diffusion (E_d) using least-squares fits of these linear plots. Similarly, the activation energies for the permeation of water (E_{pw}) and *tert*-butanol (E_{pTER}) and the diffusion of water (E_{Dw}) were estimated. The values thus obtained are presented in Table 7.

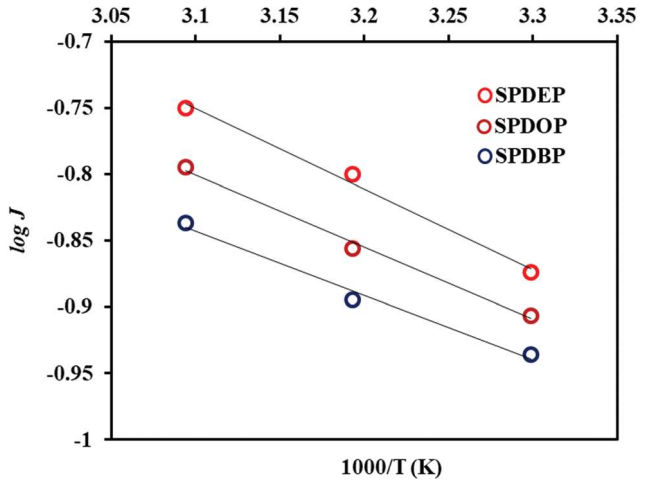

Fig. 16 Variation of log$J$ with temperature for different plasticizer incorporated membranes at 10 mass% water in the feed.

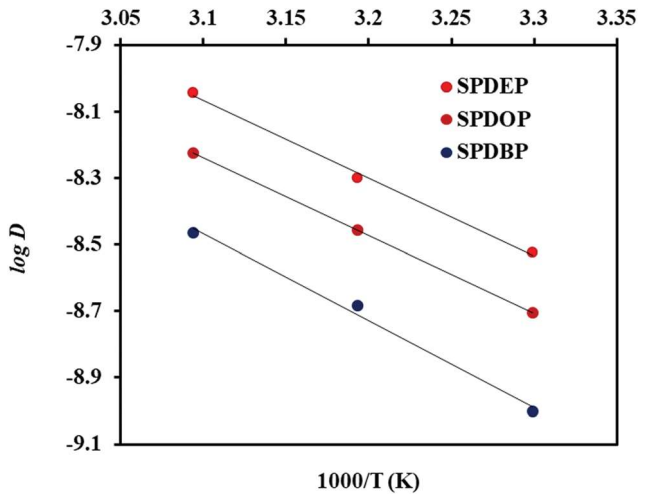

Fig. 17 Variation of log$D$ with temperature for different plasticizer incorporated membranes at 10 mass% water in the feed.

Table 7 Arrhenius activation parameters for permeation and diffusion and heats of sorption of plasticizer incorporated membranes

Parameter (kJ mol^{-1})	SPDEP	SPDBP	SPDOP
E_p	9.34	12.40	12.65
E_D	9.77	13.01	13.34
E_{pw}	9.28	12.33	12.57
E_{pTER}	49.13	55.86	69.37
E_{Dw}	9.72	12.95	13.26
ΔH_s	−0.43	−0.61	−0.69

From Table 7, it is observed that the apparent activation energy values of water (E_{pw}) are much lower than those of *tert*-butanol (E_{pTER}), suggesting that the membranes developed with the different plasticizers demonstrated excellent separation efficiency towards water. The activation energy values for permeation of water (E_{pw}) and total permeation (E_p) are close to each other, signifying that the coupled transport of both water and *tert*-butanol molecules is minimal because of the higher selective nature of the membranes towards water. The E_p values of *tert*-butanol and water ranged between 49.13 and 69.37 kJ mol^{-1} and 9.28 and 12.57 kJ mol^{-1}, respectively. The estimated E_p and E_D values ranged between 12.65 and 9.34 kJ mol^{-1} and 13.34 and 9.77 kJ mol^{-1}, respectively. Using these values, we calculated the heat of sorption using eqn (11).

$$\Delta H_s = E_p - E_D \quad (11)$$

The resulting ΔH_s values are included in Table 7. It is noticed that the ΔH_s values obtained in the present study are negative for all the membranes, suggesting that Langmuir's mode of sorption is predominant, giving an exothermic contribution.

Conclusions

In the present study, different plasticizer incorporated cross-linked NaAlg/PSSAMA membranes were prepared by employing a solution casting technique. Among the developed membranes, the DEP incorporated NaAlg/PSSAMA membrane demonstrated an excellent permeation flux and separation factor. This was explained on the basis of the significant enhancement of hydrophilicity, establishment of hydrogen bonding, chain flexibility and electrostatic interaction in the membrane matrix. The DEP containing membrane showed the highest separation factor of 12 830 with a flux of 1.306 × 10^{-3} kg m^{-2} h^{-1} at 10 mass% water in the feed at 30 °C. Experimental data also revealed that the total flux and the flux of water overlap with each other, particularly for the DEP incorporated membrane, suggesting that the developed membrane with DEP was highly selective towards water and this is in good agreement with the diffusion data. All the membranes showed lower activation energy values for water (E_{pw}) than for *tert*-butanol (E_{pTER}), suggesting that the plasticizer incorporated membranes have higher separation efficiency. All the obtained ΔH_s values are negative, indicating that Langmuir's mode of sorption is predominant for all the membranes. Based on

these results, it is concluded that the DEP incorporated membrane could be a potential candidate for industrial separation of water/*tert*-butanol.

Nomenclature

M_w	Molecular weight
A	Effective membrane area (m^2)
D_S	Degree of swelling (%)
D_o	Pre-exponential factor for diffusion
E_D	Activation energy for diffusion (kJ mol^{-1})
E_{Dw}	Activation energy for diffusion of water (kJ mol^{-1})
E_p	Activation energy for permeation (kJ mol^{-1})
E_{pw}	Activation energy for permeation of water (kJ mol^{-1})
E_{pTBOH}	Activation energy for permeation of *tert*-butanol
E_x	Activation energy for permeation or diffusion (kJ mol^{-1})
ΔH_s	Heat of sorption (kJ mol^{-1})
J	Total flux (kg m^{-2} h^{-1})
J_o	Pre-exponential factor for permeation
PSI	Pervaporation separation index
P and F	Mass percents of the permeate and feed
R	Gas constant
t	Permeation time (h)
T	Temperature (K)
W	Mass of permeate (kg)
W_s and W_d	Masses of the swollen and dry membranes

Greek letters

δ	Membrane thickness (40 μm)
$\propto_{sep}$	Separation factor

Conflicts of interest

No conflicts to declare.

Acknowledgements

The authors wish to thank the Department of Science & Technology, New Delhi, for extending the financial support under the DST-PURSE-Phase-II Program [Grant No. SR/PURSE PHASE-2/13(G)].

References

1 P. D. Chapman, T. Oliveira, A. G. Livingston and K. Li, *J. Membr. Sci.*, 2008, **1–2**, 5–37.
2 H. Chang, Y. Wang, L. Xiang, D. H. Liu, C. Q. Wang and Y. C. Pan, *Chem. Eng. Sci.*, 2018, **192**, 85–93.
3 C. Castel, L. Wang, J. P. Corriou and E. Favre, *Chem. Eng. Sci.*, 2018, **183**, 136–147.
4 M. Ulbricht, *Polymer*, 2006, **7**, 2217–2262.
5 H. X. Liu, N. X. Wang, C. Zhao, S. L. Ji and J. R. Li, *Chin. J. Chem. Eng.*, 2018, **26**, 1–16.
6 F. J. Novita, H. Y. Lee and M. Y. Lee, *Chem. Eng. Sci.*, 2018, **190**, 297–311.
7 T. Wang, Y. Zhang, X. Shi, L. Wu, X. Zhang and S. Zhang, *Chem. Eng. Sci.*, 2019, **201**, 191–200.
8 T. Gallego-Lizon, E. Edwards, G. Lobiundo and L. F. dos Santos, *J. Membr. Sci.*, 2002, **197**, 309–319.
9 S. Biduru, S. Sridhar, G. S. Murthy and S. Mayor, *J. Chem. Technol. Biotechnol.*, 2005, **80**, 1416–1424.
10 P. Shao and R. Y. M. Huang, *J. Membr. Sci.*, 2007, **2**, 162–179.
11 P.-Y. Zheng, C.-C. Ye, X.-S. Wang, K.-F. Chen, Q.-F. An, K.-R. Lee and C.-J. Gao, *J. Membr. Sci.*, 2016, **510**, 220–228.
12 K. Huang, G. Liu, J. Shen, Z. Chu, H. Zhou, X. Gu, W. Jin and N. Xu, *Adv. Funct. Mater.*, 2015, **36**, 5809–5815.
13 B. Bolto, T. Tran, M. Hoang and Z. Xie, *Prog. Polym. Sci.*, 2009, **9**, 969–981.
14 B. B. Munavalli, S. R. Naik and M. Y. Kariduraganavar, *Electrochim. Acta*, 2018, **286**, 350–364.
15 S. Xu and Y. Wang, *J. Membr. Sci.*, 2015, **496**, 142–155.
16 G. Dudek, M. Krasowska, R. Turczyn, A. Strzelewicz, D. Djurado and S. Pouget, *Chem. Eng. Res. Des.*, 2019, **144**, 483–493.
17 B. B. Munavalli, A. I. Torvi and M. Y. Kariduraganavar, *Polymer*, 2018, **142**, 293–309.
18 Q. Zhao, Q. F. An, Y. Ji, J. Qian and C. Gao, *J. Membr. Sci.*, 2011, **1**, 19–45.
19 K.-F. Chen, P.-Y. Zheng, J.-K. Wu, N.-X. Wang, Q.-F. An and K.-R. Lee, *J. Membr. Sci.*, 2018, **545**, 284–291.
20 X. Zhang, M. Wang, C.-H. Ji, X.-R. Xu, X.-H. Ma and Z.-L. Xu, *Sep. Purif. Technol.*, 2018, **203**, 84–92.
21 Q. F. An, J. W. Qian, Q. Zhao and C. J. Gao, *J. Membr. Sci.*, 2008, **313**, 60–67.
22 G. J. Zhang, X. Song, S. L. Ji, N. X. Wang and Z. Z. Liu, *J. Membr. Sci.*, 2008, **325**, 109–116.
23 S. Kalyani, B. Smitha, S. Sridhar and A. Krishnaiah, *Carbohydr. Polym.*, 2006, **64**, 425–432.
24 S. Kalyani, B. Smitha, S. Sridhar and A. Krishnaiah, *Desalination*, 2008, **229**, 68–81.
25 H. H. Tønnesen and J. Karlsen, *Drug Dev. Ind. Pharm.*, 2002, **6**, 621–630.
26 P. Kanti, K. Srigowri, J. Madhuri, B. Smitha and S. Sridhar, *Sep. Purif. Technol.*, 2004, **3**, 259–266.
27 S. D. Bhat and T. M. Aminabhavi, *Sep. Purif. Rev.*, 2007, **3**, 203–229.
28 K. B. Narayanan and S. S. Han, *Food Chem.*, 2017, **234**, 103–110.
29 H.-R. Xie, C.-H. Ji, S.-M. Xue, Z.-L. Xu, H. Yang and X.-H. Ma, *Sep. Purif. Technol.*, 2018, **206**, 218–225.
30 W. Zhang, C. Pan, Q. Ge, L. Zhang and X. Wang, *J. Membr. Sci. Res.*, 2017, **3**, 272–280.
31 D. Anjali Devi, B. Smitha, S. Sridhar and T. M. Aminabhavi, *J. Membr. Sci.*, 2005, **1–2**, 91–99.
32 X. H. Ma, Z. L. Xu, C. Q. Ji, Y. M. Wei and H. Yang, *J. Appl. Polym. Sci.*, 2011, **2**, 1017–1024.
33 D. Kim, H. B. Park, J. W. Rhim and Y. M. Lee, *J. Membr. Sci.*, 2004, **240**, 37–48.
34 P. S. Rachipudi, A. A. Kittur, A. M. Sajjan, R. R. Kamble and M. Y. Kariduraganavar, *Chem. Eng. Sci.*, 2013, **94**, 84–92.

35 P. Jia, L. Hu, G. Feng, C. Bo, M. Zhang and Y. Zhou, *Mater. Chem. Phys.*, 2017, **190**, 25–30.
36 H. Kang, Y. Li, M. Gong, Y. Guo, Z. Guo, Q. Fang and X. Li, *RSC Adv.*, 2018, **8**, 11643–11651.
37 Y. Xue, C. H. Lau, B. Caoa and P. Li, *J. Membr. Sci.*, 2019, **575**, 135–146.
38 N. A. Peppas and L. B. Peppas, *J. Food Eng.*, 1994, **22**, 189–210.
39 D. Achari, P. Rachipudi, S. Naik, R. Karuppannan and M. Kariduraganavar, *J. Ind. Eng. Chem.*, 2019, **78**, 383–395.
40 R. W. Baker, J. G. Wijmans and Y. Huan, *J. Membr. Sci.*, 2010, **348**, 346–352.
41 A. S. Kulkarni, S. M. Badi, A. M. Sajjan, N. R. Banapurmath, M. Y. Kariduraganavar and A. S. Shettar, *Chemical Data Collections*, 2019, **22**, 100245–100261.
42 Q. F. An, J. W. Qian, H. B. Sun, L. N. Wang, L. Zhang and H. L. Chen, *J. Membr. Sci.*, 2003, **222**, 113–122.
43 X. Zhang and Z. Chen, *Langmuir*, 2014, **30**, 4933–4944.
44 M. Rezayi, L. Y. Heng, A. Kassim, S. Ahmadzadeh, Y. Abdollahi and H. Jahangirian, *Sensors*, 2012, **12**, 8806–8814.
45 P. Das and S. K. Ray, *J. Ind. Eng. Chem.*, 2016, **34**, 321–336.
46 B. Sarker, D. G. Papageorgiou, R. L. Silva, T. Zehnder, F. Gul-E-Noor, M. Bertmer, J. Kaschta, K. Chrissafis, R. Detscha and A. R. Boccaccini, *J. Mater. Chem. B*, 2014, **2**, 1470–1482.
47 B. H. Nanjunda Reddy, P. Ranjan Rauta, V. Venkata Lakshmi and S. Sreenivasa, *Int. J. Appl. Pharm.*, 2018, **10**, 141–150.
48 C. M. Mathew, B. Karthika, M. Ulaganathan and S. Rajendran, *Bull. Mater. Sci.*, 2015, **38**, 151–156.
49 S. Ramesh, T. S. Yin and C. W. Liew, *Ionics*, 2011, **17**, 705–713.
50 Siddaramaiah, T. M. Mruthyunjaya Swamy, B. Ramaraj and J. H. Lee, *J. Appl. Polym. Sci.*, 2008, **109**, 4075–4081.
51 P. Jia, L. Hu, X. Yang, M. Zhang, Q. Shang and Y. Zhou, *RSC Adv.*, 2017, **7**, 30101–30108.
52 T. F. Ceia, A. G. Silva, C. S. Ribeiro, J. V. Pinto, M. H. Casimiro, A. M. Ramos and J. Vital, *Catal. Today*, 2014, **236**, 98–107.
53 T. Mekonnen, P. Mussone, H. Khalil and D. Bressler, *J. Mater. Chem. A*, 2013, **1**, 13379–13398.
54 P. S. Rachipudi, A. A. Kittur, A. M. Sajjan and M. Y. Kariduraganavar, *J. Membr. Sci.*, 2013, **441**, 83–92.
55 W. F. Guo, T. S. Chung, T. Matsuura, R. Wang and Y. Liu, *J. Appl. Polym. Sci.*, 2004, **91**, 4082–4090.
56 R. Subrahmanyam, P. Gurikov, P. Dieringer, M. Sun and I. Smirnova, *Gels*, 2015, **1**, 291–313.
57 H. Thiess, A. Schmidt and J. Strube, *Membranes*, 2018, **8**, 1–27.
58 B. Liang, Q. Li, B. Cao and P. Li, *Desalination*, 2018, **433**, 132–140.
59 P. S. Rachipudi, M. Y. Kariduraganavar, A. A. Kittur and A. M. Sajjan, *J. Membr. Sci.*, 2011, **383**, 224–234.
60 J. G. Varghese, R. S. Karuppannan and M. Y. Kariduraganavar, *J. Chem. Eng. Data*, 2010, **55**, 2084–2092.
61 P. S. Rachipudi, A. A. Kittur, S. K. Choudhari, J. G. Varghese and M. Y. Kariduraganavar, *Eur. Polym. J.*, 2009, **45**, 3116–3126.